Journal of Geodynamics 120 (2018) 1–10

Contents lists available at ScienceDirect

Journal of Geodynamics

journal homepage: www.elsevier.com/locate/jog

Crustal deformation and strain fields of the Weihe Basin and surrounding area of central China based on GPS observations and kinematic models

Wei Qu[a,b], Zhong Lu[b,*], Qin Zhang[a], Qingliang Wang[c], Ming Hao[c], Wu Zhu[a], Feifei Qu[a]

[a] College of Geology Engineering and Geomatics, Chang'an University, Xi'an, Shaanxi 710054, China
[b] Department of Earth Sciences, Southern Methodist University, Dallas, TX 75275, USA
[c] Second Monitoring Center, China Earthquake Administration, Xi'an, Shaanxi 710054, China

ARTICLE INFO

Keywords:
Crustal strain field
Weihe Basin
GPS
Kinematic model
Tectonic activity

ABSTRACT

The Weihe Basin in central China is characterized by its complex geological background and intense tectonic activity. This study examined the characteristics of the crustal deformation and strain field of the Weihe Basin and its surroundings based on campaign Global Positioning System (GPS) data acquired during 2001–2011. We first analyzed the variations of crustal movement and we calculated the crustal strain rates by establishing sound strain models. Both the characteristics of the strain field and the correlation between the maximum shear strain field and the distribution of seismicity were investigated. Our results indicated that the overall crustal movement of the Weihe Basin region was temporally continuous during 2001–2011, despite short-term fluctuation during 2007–2008. We found that western and eastern parts of the Weihe Basin region presented considerably different tectonic characteristics with predominantly compressional strain in the west and extensional strain in the east. However, the magnitude and direction of the overall crustal movement, and the relative differential motions of the Weihe Basin region, changed obviously during 2007–2008 with substantially increased compressional strain in western areas. We conclude that regions with higher shear strain are also those with frequent earthquakes, the distribution of which might have been affected by the M8.0 Wenchuan earthquake in May 2008. According to variations of the crustal deformation and the strain field, we further infer that western parts of the Weihe Basin region during 2007–2008 might have been affected by a northeastward extrusion caused by the Wenchuan earthquake. However, this dynamic effect might have gradually permeated to eastern parts of the Weihe Basin region during 2008–2011. The results obtained in this paper not only portray the current tectonic activity deformations but also the recent geodynamic processes of the Weihe Basin and its surrounding area.

1. Introduction

The Weihe Basin, located in Shaanxi Province in central China (Fig. 1a), is surrounded by the Qinghai–Tibet Block, Ordos Block, North China Block, and South China Block (Fig. 1b) (Feng et al., 2003; Dai et al., 2004; Shi et al., 2008; Qu et al., 2009, 2011; Yang et al., 2013; Rao et al., 2014; Lin et al., 2015; Gao et al., 2015; Jiang et al., 2016). The Weihe Basin and surrounding area (hereafter, referred to as the Weihe Basin region) is characterized by intense crustal activity, and it comprises is an important component of the well-known Fen–Wei Seismic Belt (Fig. 1c) (Jiang et al., 2000; Myers and Gomez, 2010; Liu et al., 2016). Therefore, the Weihe Basin region, which constitutes an important natural laboratory for the study of active tectonic deformation in a typical intracontinental graben system, has attracted considerable attention from many researchers in the field of geoscience.

Recent geophysical, geological, and geodetic studies have revealed various important aspects of the Weihe Basin region. Its crustal structure has been studied based on geological investigations (Wang et al., 2014), and its orogenic tectonic movement has been investigated through the analysis of rock samples (Chen et al., 2015). The tectonic activities and structural features of the active faults of the Weihe Basin region have been revealed by fault profiles (Shi et al., 2008), high-resolution remote sensing imagery (Rao et al., 2014), and field observations (Feng et al., 2003; Deng, 2007; Li et al., 2015; Lin et al., 2015). The earthquakes that have occurred within the basin have been studied using earthquake catalogs (Liu et al., 2016) and field investigations (Rao et al., 2014). Furthermore, the deep crustal structure and geophysical characteristics beneath the basin have been determined using seismic wave velocity (Bai et al., 2008) and seismic tomography (Pan and Niu, 2011; Ren et al., 2013; Guo and Chen, 2016). The features and mechanisms of ground fissures have been studied by interferometric synthetic aperture radar (Qu et al., 2014a), field investigations, and

* Corresponding author.
E-mail address: zhonglu@smu.edu (Z. Lu).

https://doi.org/10.1016/j.jog.2018.06.003
Received 13 May 2017; Received in revised form 27 April 2018; Accepted 17 June 2018
Available online 20 June 2018

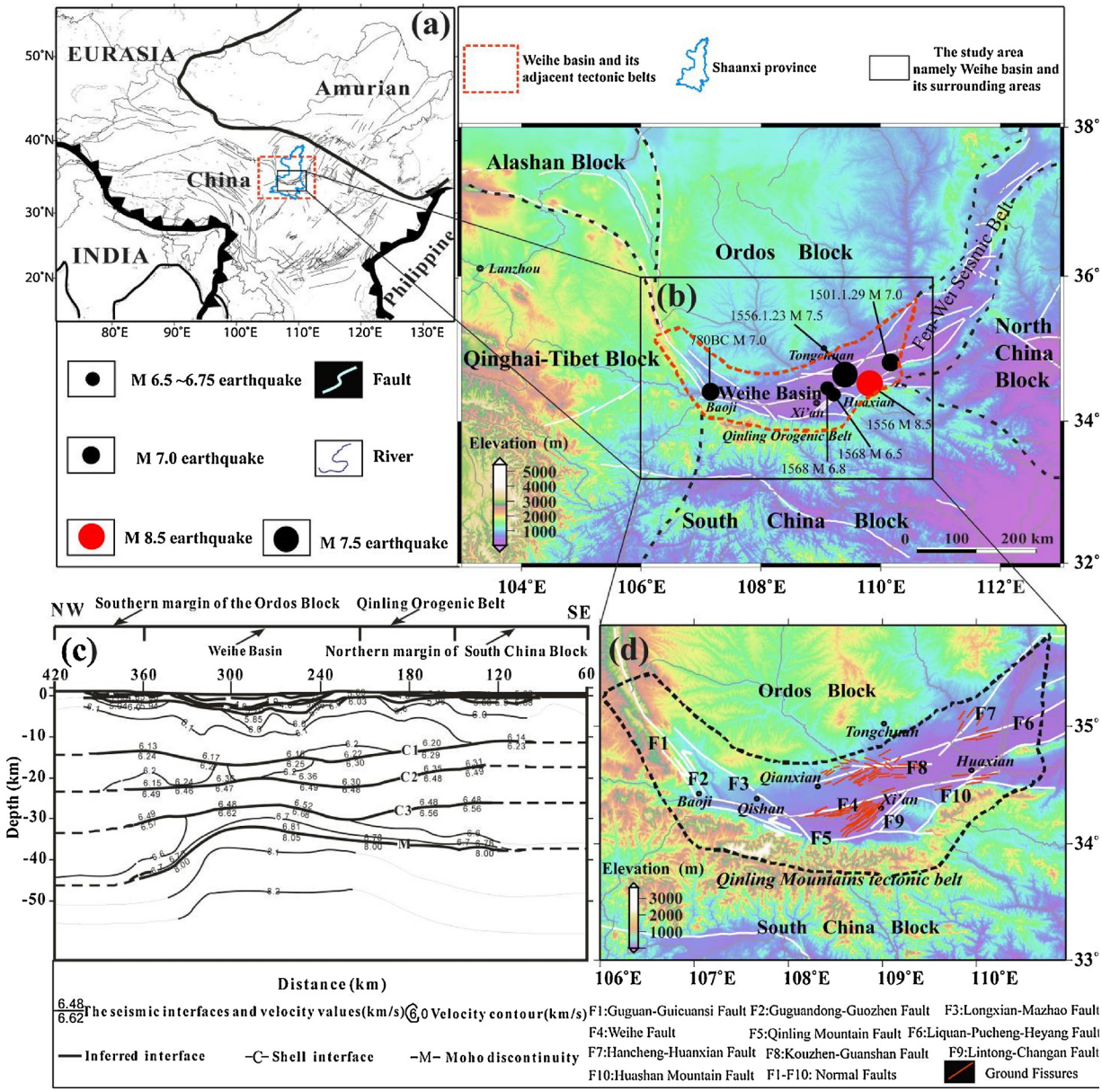

Fig. 1. Location of the Weihe basin and its surroundings in China, as well as the major plate boundaries in and near mainland China (Fig. 1a). The red dashed box indicates the Weihe basin and its adjacent tectonic belts. The black thin dotted lines indicate the division of the tectonic units and their boundaries, such as the Qinghai-Tibet Block, the Ordos Block, the North China Block and the South China Block. The blue closed outline represents the whole Shaanxi province. The black rectangular box is the specific location of the study area: the Weihe basin and its surrounding area (Fig. 1b). The red thick dotted lines indicate the scope of the Weihe basin determined by geological data (Peng, 1992b, Fig. 1b). The white solid lines represent the major active faults (Zhang et al., 2005). The small double circles represent the major cities. The light blue curves represent the rivers. The solid filled circles (black and/or red) of varying size indicate the epicenters and magnitude of the large historical earthquakes within the Weihe basin region (Lin et al., 2015). Fig. 1c shows the stratigraphy of the Weihe basin obtained from the wide-angle reflection method (Ren et al., 2012). Fig. 1d shows the distribution of major faults within the Weihe basin. F1-F10 represent the numbers and names of these major faults (Zhang et al., 2012). The red solid lines represent ground fissures within the Weihe basin (Zhang et al., 2012) (For interpretation of the references to colour in this figure legend, the reader is referred to the web version of this article).

mechanical simulations (Peng et al., 2013). The tectonic stress field and structural extension of the Weihe Basin region have been modeled using numerical simulations (Zhang et al., 2011), kinematic analysis of faults (Mercier et al., 2013), field observations and thermochronology (Liu et al., 2013). Moreover, the crustal deformations and tectonic movements have been analyzed based on Global Positioning System (GPS) observations (Dai et al., 2004; Qu et al., 2011; Zhang et al., 2012; Cui et al., 2016).

Previous studies that have applied different methods to investigate the crustal deformations and tectonic characteristics of the Weihe Basin region constitute important references for the regional geodynamics. Among the abovementioned methods, GPS technology has been proven especially useful for studying crustal deformation and geodynamic processes. Although GPS data have been used to describe the general characteristics of the crustal motion of the entire Weihe Basin region, there has been a lack of detailed study on the variations of relative motions and strain fields within the basin. Variations of both the GPS velocities and the crustal strain fields are useful not only for describing the development of tectonic activity, but also for characterizing the internal mechanisms of ongoing basin deformation. Moreover, variations of relative differential velocities can reflect more clearly the interior motions of the basin.

This study used GPS data from the Weihe Basin region, which were acquired during different periods by the Seismological Bureau of Shaanxi Province and the Crustal Movement Observation Network of China. The objectives were to investigate the variations of crustal velocity fields and relative differential motions within the basin, and to explore the variations of crustal strain fields through establishing sound strain models. Finally, the variations of the strain fields, as well as the correlation between the maximum shear strain field and seismicity, were examined.

2. General tectonic background

The Weihe Basin is a Cenozoic rift basin that is one of the intracontinental graben systems around the Ordos Block in central China (Fig. 1a) (Zhang et al., 1998). The basin is bounded by the Qinghai–Tibet Block to the west, stable Ordos Block to the north, North China Block to the east, and Qinling Orogenic Belt and South China Block to the south (Lin et al., 2015). The Weihe Basin is irregular in shape, being narrower in the west along the Weihe River (Lin et al., 2015), and it connects with the Shanxi Graben in the east (Fig. 1b). Since the Eocene, the basin has received sedimentary deposits up to 7000-m thick due to the uplift of mountainous blocks to the south and north of the basin (SSB, 1988; Zhang et al., 1998; Lin et al., 2015).

Geological and geophysical data indicate that many active normal faults have developed in the Weihe Basin region (e.g., Peng, 1992a; Feng et al., 2003; Tian et al., 2003; Deng, 2007; Shi et al., 2008). In southeastern parts, normal faults are characterized by a series of stepped fault scarps dipping into the basin with an average dip-slip rate of ~2 mm/yr (Rao et al., 2014; Lin et al., 2015). The slip rates of major active faults in the northern and western parts of the basin are estimated to be of the order of 0.1–0.5 mm/yr (Xu et al., 1988). These active normal faults have developed in response to pre-existing spreading and rifting of the continental crust caused by variations in lithospheric structures with respect to the neighboring Ordos Block to the north and the Qinling Orogenic Belt to the south (Fig. 1d and e) (SSB, 1988; Bao et al., 2011; Rao et al., 2014; Lin et al., 2015).

Among more than 10 large historical earthquakes of ≥ M7.0 (including 4 of ≥ M8.0) that have occurred in the graben systems around the Ordos Block, 4 have occurred in the Weihe Basin region (SSB, 1988; Deng, 2007). The most devastating earthquake was the 1556 M8.5 Huaxian earthquake in the eastern part of the Weihe Basin, which devastated 130 counties in 11 provinces and caused more than 830,000 fatalities (e.g., Kuo, 1957; Wang, 1980; SSB, 1988; Xie, 1992; CENC, 2007; Liu and Wang, 2012). Other strong earthquakes that have occurred within the Weihe Basin region include the 780 BCE M7.0 Baoji earthquake, 1501 M7.0 Chaoyi earthquake, 1556 M7.5 Yanliang earthquake, 1568 M6.8 Lintong earthquake, and 1568 M6.5 Gaoling earthquake (Lin et al., 2015) (Fig. 1c). High levels of historical seismicity and the associated focal mechanisms indicate that normal faulting in the Weihe Basin has been seismically active under the intracontinental extensional regime (e.g., SSB, 1988; Zhang et al., 1998; Deng, 2007; Rao et al., 2014; Lin et al., 2015). Most importantly, the Weihe Basin region not only has history of strong earthquakes but it also has recent high frequency of tectonic activity (Qu et al., 2011; Lin et al., 2015).

3. GPS data and crustal movements

3.1. Distribution of GPS velocity fields

The main purpose behind the construction of the Crustal Movement Observation Network of China GPS monitoring network was to investigate the crustal movements and deformations of the Weihe Basin region and the surrounding areas (SMCCEA, 2013). This GPS network consists of approximately 35 campaign GPS sites that have been occupied annually and observed for at least 3 days during each survey. The GPS velocities used in the study were provided by the Second Monitoring Center of the China Earthquake Administration (SMCCEA, 2013), who processed the GPS data using the GAMIT/GLOBK software packages (King and Bock, 2000; Herring, 2002), based on the processing strategy used in both Shen et al. (2000) and Wang (2009). The station positions and velocities were estimated in the ITRF2008 reference frame (Altamimi et al., 2011) using the quasi-observation combination analysis technique (Dong et al., 1998, 2006). As the focus of this study was on the analysis of the interior crustal deformation of the Weihe Basin region, the GPS velocity solutions were further transformed into a regional reference frame with respect to the Eurasian Plate. The Eurasian Plate is a stable block located in the northwest of mainland China (Fig. 1a; Qu et al., 2014b; Kogan et al., 2000). The Euler vector of the Eurasian Plate was calculated by applying constraints that minimize the motions at 11 IGS stations distributed within the stable interiors in the ITRF2008 reference frame (SMCCEA, 2013; Wang, 2009; Shen et al., 2000). Then, the GPS velocity solutions of the Weihe Basin region with respect to the Eurasian Plate were obtained based on the Euler vector of the Eurasian plate (SMCCEA, 2013; Wang, 2009; Shen et al., 2000). The horizontal components of the GPS velocity fields together with the 95% confidence error ellipses for the periods 2001–2007 and 2008–2011 are shown in Fig. 2a and b, respectively. In addition, to investigate the change in the deformation field of the study area during the one-year period prior to the nearby May 2008 M8.0 Wenchuan earthquake (~500 km to the southwest of the study area) (Xu et al., 2010), GPS velocity fields were calculated for the period 2007–2008 (Fig. 2c). Because the 2008 GPS campaigns were conducted during mid-September, the coseismic effect of the Wenchuan earthquake was removed from the velocity field for the period 2007–2008 using the coseismic displacement field (Shen et al., 2009; SMCCEA, 2013).

Comparison of the GPS velocity field of 2001–2007 (Fig. 2a) with 2008–2011 (Fig. 2b) revealed that the entire basin had an overall tendency of movement toward the southeast with respect to the stable Eurasian Plate, which fits into the geodynamic setting of the study area (Qu et al., 2014b; Shen et al., 2009; Gan et al., 2007). The main difference is that the direction of the GPS velocity field during 2008–2011 was deflected slightly toward the east and its magnitude was slightly larger (Fig. 2b versus a). However, during 2007–2008, both the magnitude and the direction of the crustal velocity changed, especially in western and central parts of the Weihe Basin region (Fig. 2c); the magnitude was largest during 2001–2011, while the direction changed from southeastward to northeastward. Nevertheless, the overall crustal movement of the Weihe Basin region appears to have been recovering during 2008–2011, despite the short-term fluctuation (2007–2008). These features indicate that the overall crustal movement of the Weihe Basin region was temporally continuous during the observation period (2001–2007 and 2008–2011).

3.2. Differential motion fields within Weihe Basin region

Relative to the stable Eurasian Plate, the velocity field of the Weihe Basin region includes a rigid rotational component and a spatially varying component within the basin. To analyze further the interior motions within the Weihe Basin region, we calculated the differential motion field by removing the rigid rotation of the entire study area based on the solution from the Euler vector (Gan et al., 2007). The residual velocity fields (Fig. 2d–f) allow us to appreciate the spatially varying differential motions inside the basin. Additionally, because the velocity field is a vector field, the differential motion field is the vector difference. When the rigid rotation velocity is removed from the velocity field relative to the stable Eurasian Plate, the differential velocities of the GPS sites can present different directions. It should be noted that, because of the limited number of GPS sites within the basin, the trend of the differential motion field does not appear uniform. However, the strength of the crustal motions within the Weihe Basin region can be

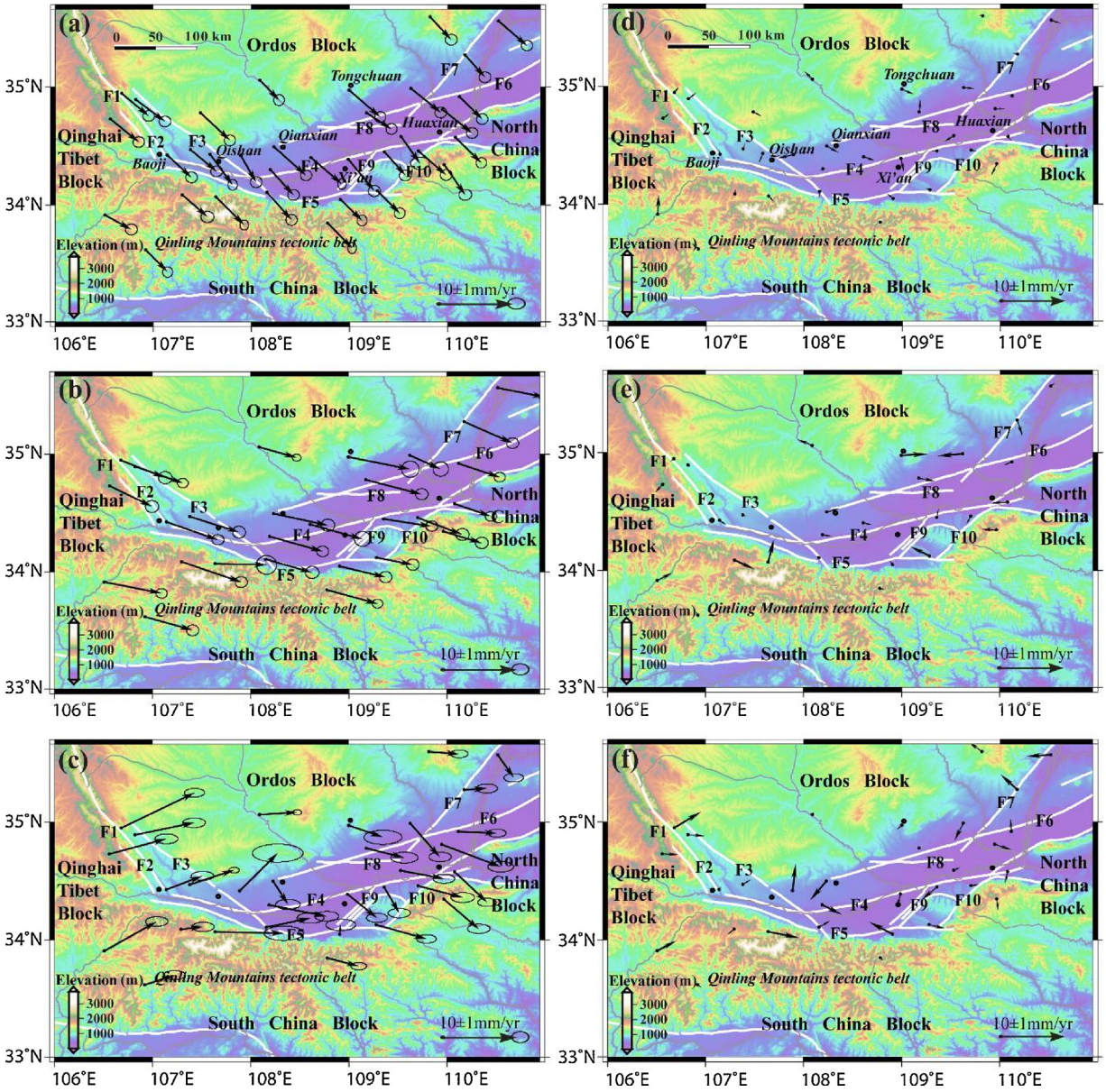

Fig. 2. The GPS velocities of the Weihe basin region for the periods of 2001–2007 (Fig. 2a), 2008–2011 (Fig. 2b) and 2007–2008 (Fig. 2c), respectively (unit: mm/yr). Solid black arrows are GPS velocities with respect to the stable Eurasia plate based on ITRF2008 reference frame. The differential velocities are for the periods of 2001–2007 (Fig. 2d), 2008–2011 (Fig. 2e) and 2007–2008 (Fig. 2f), respectively.

detected from the differential motion field; thus, the changes in differential motions during the three different periods could be revealed. We found no obvious differential motion between the western and eastern parts during 2001–2007 and the magnitudes of the velocities were all small, i.e., averaging ~1.3 mm/yr (Fig. 2d). During 2008–2011, differential motions between the western and eastern parts did exist; the interior crustal activities were relatively larger in eastern parts than western parts (Fig. 2e). However, we found that the overall magnitude of interior movement of the Weihe Basin region increased considerably during 2007–2008 (Fig. 2f).

4. Strain model and significance testing

4.1. Strain model

The spatial characteristics of the crustal GPS velocity field can reveal the crustal deformation, although the reference frame might have an influence (Ward, 1994; Wu et al., 2015). Unlike velocity data, the strain rate is independent of the frame of reference. In addition, the strain rate field can describe numerically the ongoing geodynamic processes, reflect the response of the internal mechanism(s) of crustal deformation, and reveal local strain accumulation rates and their possible correlation with seismicity (Ward, 1994; Calais et al., 2000; Hori, 2003; Hackl et al., 2009; Riguzzi et al., 2012). Therefore, we used GPS observations at different periods to establish sound crustal strain models.

We employed the kinematic model (Eq. 1) to model the variations of the strain fields of the Weihe Basin. Actually, the kinematic model (Eq. 1) is the elastic motion equation that describes the total rotation and linear strain of crustal movement. This model is derived through three steps. First, in the traditional theory of plate tectonics, a block is considered a rigid body. Therefore, according to the Euler theorem for a rigid block, the block kinematic model can be defined by the Euler equation. Second, because many reports have demonstrated that some blocks are not entirely rigid (Burbidge, 2004; Nanjo et al., 2005), deformation exists not only over the boundary zones between the blocks

but also within blocks. Hence, the crustal motion of any GPS point within a block represents the superposition of the block rotation and the differential deformation within the block. If the differential motion (or strain) within a block is homogeneous, the compound velocity vector of a point within a block can be described by the total rotation and the homogeneous strain model. Third, if the strain is uneven within a block, it can be considered a linear function of location. Therefore, there is need to model the variable strain within the block. Then, the total motion of any point within a block can be obtained by including the motion due to the rigid rotation and the motion due to the uneven strain within a block, which is the total rotation and linear strain model (Eq. 1). Detailed descriptions of Eq. (1) can be found in Qu et al. (2014b):

$$\begin{bmatrix} V_e \\ V_n \end{bmatrix} = \begin{bmatrix} -r\sin\varphi\cos\lambda & -r\sin\varphi\sin\lambda & r\cos\varphi \\ r\sin\lambda & -r\cos\lambda & 0 \end{bmatrix} \begin{bmatrix} \omega_x \\ \omega_y \\ \omega_z \end{bmatrix} + \begin{bmatrix} A_0 & B_0 \\ B_0 & C_0 \end{bmatrix} \begin{bmatrix} x \\ y \end{bmatrix} + \frac{1}{2} \begin{bmatrix} \xi_1 & \xi_2 \\ \zeta_1 & \zeta_2 \end{bmatrix} \begin{bmatrix} x^2 \\ y^2 \end{bmatrix} + \begin{bmatrix} \xi_3 \\ \zeta_3 \end{bmatrix} xy, \tag{1}$$

where V_e and V_n are the eastern and northern components of the velocity vector of any point within the study region, respectively; (λ, φ) are the longitude and latitude of the point; r is the average radius of the Earth; ω_x, ω_y, and ω_z are the components of the Euler vector; (x, y) are the coordinates of the point in the spherical coordinate system (Savage et al., 2001; Reddy, 2013; Wu et al., 2015); and A_0, B_0, C_0, ξ_1, ξ_2, ξ_3, ζ_1, ζ_2, and ζ_3 are the strain parameters. Here, A_0, B_0, and C_0 are the linear terms of the strain parameters that describe the homogeneous strain features, and the terms ξ_1, ξ_2, and ξ_3 and ζ_1, ζ_2, and ζ_3 are the quadratic terms of the strain parameters that characterize the uneven strain features.

4.2. Applicability and significance testing

Errors in GPS measurements could affect the calculated strain parameters in the kinematic model. Statistical significance hypothesis testing can minimize the GPS errors and provide realistic strain parameters for characterizing the crustal deformation features of the Weihe Basin region. In this study, we performed significance hypothesis testing on the quadratic terms of the strain parameters in Eq. (1), which can fully represent the nature of the uneven strains. Then, from a statistical point of view, we could determine the quadratic terms of the strain parameters as true or false under the given significance level. Accordingly, Eq. (1) can be expressed in matrix form as follows:

$$\underset{2\times1}{V} = \underset{2\times66\times1}{A}\ \underset{}{X} + \underset{2\times66\times1}{B}\ \underset{}{Y}, \tag{2}$$

where:

$$A = \begin{bmatrix} -r\sin\varphi\cos\lambda & -r\sin\varphi\sin\lambda & r\cos\varphi & r(\lambda-\lambda_0)\cos\varphi & r(\varphi-\varphi_0) & 0 \\ r\sin\lambda & -r\cos\lambda & 0 & 0 & r(\lambda-\lambda_0)\cos\varphi & r(\varphi-\varphi_0) \end{bmatrix}, \tag{3}$$

$$X = [\omega_x\ \ \omega_y\ \ \omega_z\ \ A_0\ \ B_0\ \ C_0]^T, \tag{4}$$

$$B = \begin{bmatrix} x^2 & y^2 & xy & 0 & 0 & 0 \\ 0 & 0 & 0 & x^2 & y^2 & xy \end{bmatrix},\ Y = [\xi_1\ \ \xi_2\ \ \xi_3\ \ \zeta_1\ \ \zeta_2\ \ \zeta_3]^T. \tag{5}$$

Eq. (2) can be regarded as an adjustment model with additional system parameters; vector X consists of the main parameters of the equation including the Euler vector and the linear terms of the strain parameters, while vector Y is the added system parameter consisting of the quadratic terms of the strain parameters.

Eq. (2) can be further rewritten as follows by applying the method of linear hypothesis testing (Koch, 1980; Tao, 2007):

$$\begin{cases} \Delta_{2n\times1} = \overline{A} \begin{bmatrix} X_{6\times1} \\ Y_{6\times1} \end{bmatrix} - l,\ \overline{A} = (A_{2n\times6},\ B_{2n\times6}) \\ H \begin{bmatrix} X \\ Y \end{bmatrix} = 0,\ H = (0_{6\times6},\ I_{6\times6}) \end{cases}, \tag{6}$$

where the linear hypothesis is H_0:$Y = 0$, Δ is the residual error of the velocity component, $l = \begin{bmatrix} V_e \\ V_n \end{bmatrix}$, n is the number of GPS stations in the study region, and I is the identity matrix.

After H_0 is set up, the F test is constructed as:

$$F = \frac{R/rank(H)}{T/(2n - rank(\overline{A}))} \sim F_{(rank(H),2n-rank(\overline{A}))}. \tag{7}$$

That is,

$$\frac{\hat{Y}^T Q_{\hat{Y}\hat{Y}}^{-1} \hat{Y}/6}{T/(2n-12)} \sim F_{(6,2n-12)}. \tag{8}$$

The reject region is:

$$F > F_{(\alpha,6,2n-12)}, \tag{9}$$

where *rank*(·) in Eq. (7) is the rank of H, $Q_{\hat{Y}\hat{Y}}^{-1}$ in Eq. (8) is the inverse of the weighting matrix for $\hat{Y}$, T in Eq. (8) is the sum of the residual squares, and α in Eq. (9) is the given significance level.

If H_0 is rejected under a significance level of α, it is reasonable to consider that the quadratic terms of the strain parameters are significant. If H_0 is accepted (i.e., Eq. (9) is false), it can be considered that the quadratic terms of the strain parameters are not significant. Using the GPS observations, we conducted linear hypothesis tests to determine the significance of the quadratic terms of the strain parameters (Table 1). It can be seen from Table 1 that the null hypothesis was rejected for the periods 2001–2007, 2008–2011, and 2007–2008, and that the F values for the three periods are all larger than the reference critical value. These findings indicate that the quadratic terms of the strain parameters were all relatively significant under a significance level of $\alpha = 0.1$. Thus, Eq (1) can be considered a reasonable model with which to represent the deformation–strain characteristics of the Weihe Basin region.

5. Results and discussions

To obtain the principal strain axes and the maximum shear strain rates, we first calculated the strain parameters (A_0, B_0, C_0, ξ_1, ξ_2, ξ_3, ζ_1, ζ_2, and ζ_3) using the total rotation and linear strain model (Eq. 1) based on the GPS velocity fields shown in Fig. 2a–c. Then, we calculated the linear and shear strains in the east–west and the north–south directions, respectively (Li et al., 2007). The maximum shear strain rates and the principal strain rates could be obtained based on the linear and shear strains. Finally, we obtained the principal strain rates (including their directions) at each GPS site in the Weihe Basin based on Eq. (1) (Li et al., 2007; Qu et al., 2014b).

5.1. Variations of the principal strain fields and their evolution tendency

Vector maps of the principal strain rates at each GPS site in the Weihe Basin region for the periods 2001–2007, 2008–2011, and

Table 1
Significance hypothesis testing of the quadratic terms of strain parameters of the Weihe basin region during the different periods.

Time periods	F value	Reference critical value (significance level$\alpha = 0.1$)	Result
2001–2007	6.02	1.87	Reject
2008–2011	2.20	1.90	Reject
2007–2008	2.23	1.89	Reject

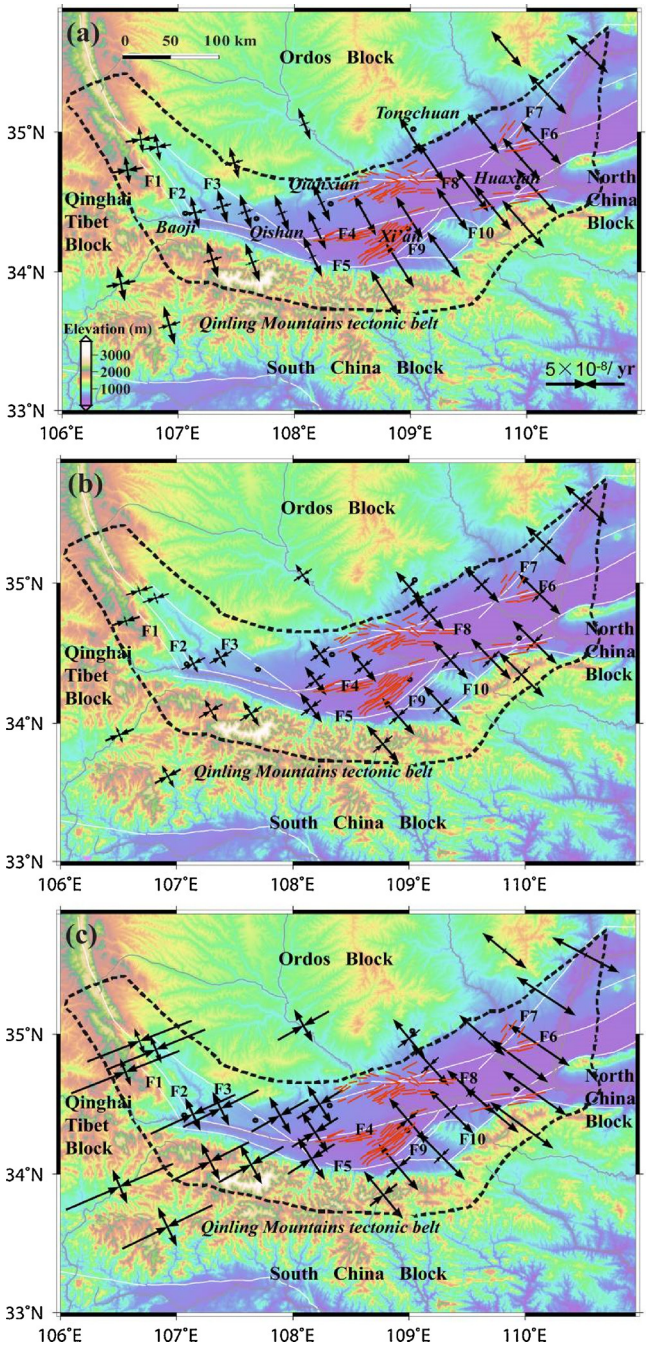

Fig. 3. Vector maps of the principal strain rates of the Weihe basin region for the periods of 2001–2007 (Fig. 3a), 2008–2011 (Fig. 3b) and 2007–2008 (Fig. 3c), respectively (unit:10^{-8}/yr). The black cross arrows indicate the principal strain rate vectors. The length and the direction of the arrow represent the magnitude and the principal direction of the principal strain rate, respectively. The opposite arrow represents the extensional principal strain rate, while the crossed arrow represents the compressional principal strain rate. The black thick dotted lines indicate the scope of the Weihe basin (Peng, 1992b).

2007–2008 are shown in Fig. 3a–c, respectively.

The spatial features of the principal strain fields during 2001–2007 (Fig. 3a) and 2008–2011 (Fig. 3b) were found similar; western parts of the Weihe Basin region possessed certain compressional strain rates, while eastern areas displayed significant extensional strain rates. However, some differences in the principal strains existed between the two periods. During 2001–2007 (Fig. 3a), the compressional strain rates in the western Weihe Basin region mainly presented in the NEE–SWW direction with a mean strain rate of about -0.9×10^{-8} /yr, whereas they were deflected slightly northward with a mean strain rate of about -1.2×10^{-8} /yr during 2008–2011 (Fig. 3b). Comparison of Fig. 3a and 3b reveals that the magnitude of the extensional strain rates in the western Weihe Basin region decreased from 2001 to 2007 to 2008–2011, as indicated by the relatively shorter black arrows. Central and eastern parts of the Weihe Basin region mainly presented extensional strain rates in the NW–SE direction (Fig. 3a). Although these areas mainly displayed extensional strain in the NW–SE direction during 2008–2011, the compressional strain rates increased over the 2001–2007 level. However, during 2007–2008, western parts of the Weihe Basin region mainly presented compressional strain rates in the approximate NE–SW direction (Fig. 3c versus a and b), with a mean compressional strain rate of about -4.4×10^{-8} /yr. The compressional strain rates in central parts of the Weihe Basin region also increased during 2007–2008 (Fig. 3c versus a). In contrast, eastern parts of the Weihe Basin region mainly presented significant and increased extensional strain in the NW–SE direction, with the extensional strain axes deflected counterclockwise by ~13° from the orientation during 2001–2007 (Fig. 3c versus a).

According to the variation characteristics of the principal strain fields, we conclude that despite the variations of the principal strain rates of the Weihe Basin region, especially in western parts during 2007–2008, the general features of the principal strain fields remained unchanged during the long term (Fig. 3b versus a). In addition, in accordance with the considerably increased compressional strain in the NE–SW direction in western parts during 2007–2008 (Fig. 3c), we further infer northeastward extrusion of the crust attributable to the May 2008 Wenchuan earthquake. Furthermore, this dynamic effect might have gradually permeated to eastern parts of the Weihe Basin region during 2008–2011, causing increased compressional strain rates and relatively intensive interior motions (Fig. 3b and e).

Relatively significant compressional strain in the NE–SW direction was predominant over the western Weihe Basin region, while obvious extensional strain in the NW–SE direction prevailed over the eastern Weihe Basin region (Fig. 3a–c). This feature is consistent with the stress–strain characteristics of the Weihe Basin region simulated using the finite element model based on geological and geophysical surveys (Zhang et al., 2011). The numerical simulation results showed that the western Weihe Basin mainly presents compressional strain, while central and eastern areas of the basin mainly present extensional strain in the NW–SE direction. The regional stress–strain fields inferred from small-earthquake composite focal mechanisms also showed that the dominant extensional stress–strain axis is in the NW–SE direction (in central and eastern parts of the basin), while the compressive axis is in the NE–SW direction (in the western basin) (SSB, 1988; Song, 1989; Wang, 2010). Additionally, the stress–strain fields inverted from borehole stress measurements (Xie et al., 1991) and fault slip data (Peng, 1992a) have all indicated the same characteristics as our derived strain fields.

By analyzing the formation of the Weihe Basin, we understand that the regional stress–strain field has mainly undergone three important episodes of evolution: early Tertiary, Miocene, and Pliocene–Quaternary (Zhang et al., 2003). In the early Tertiary period, i.e., the formation stage of the basin, the principal stress field presented tensile stress in the NWW–SEE direction. In the Miocene period during the development stage of the basin, the basin presented characteristics of right-lateral shearing activity. The direction of extensional stress was deflected from NW–SE to NE–SW. However, in the Pliocene–Quaternary, the basin presented characteristics of left-lateral shearing activity. The stress field of the basin mainly presented a tensile stress field in the NW–SE direction with certain compressional stress in the NE–SW direction. Therefore, after undergoing the above three important evolutionary episodes, the current tectonic deformation characteristics of the Weihe Basin were finally formed. The principal strain axes are considered to represent the current tectonic stress field (Fig. 3a–c). The

common spatial features of the principal strain axes during the different periods all show that western parts of the Weihe Basin region possessed compressional strain to some degree, while eastern areas displayed significant extensional strain. This characteristic of the principal strain axes is consistent with the recent geodynamic background of the region. The compressional strain axes acting at the western part of the Weihe Basin might be attributable to the effects of the India–Eurasia collision and the associated resistance of the Alashan and Ordos blocks (Liu et al., 2007; Bai et al., 2010; White and Lister, 2012). The collision is causing the crustal material of the Qinghai–Tibet Plateau to move toward the east (Bai et al., 2010). The encounter of the eastward-moving crust with the Alashan and Ordos blocks results in a compressional regime in western parts of the Weihe Basin region. In central and eastern parts of the Weihe Basin region, the prevailing extensional strain axes might be attributable to eastward slab rollback (Schellart et al., 2007; Royden et al., 2008), reduction in the rate of Pacific–Eurasia plate convergence (Northrup et al., 1995), or subduction of the Philippine Sea Plate from the southeast (Wakita et al., 2013). The result of these dynamic effects is the eastward expansion of mainland China (Zhang et al., 1998, 2003; Wang et al., 2012; Zhou et al., 2015; Li et al., 2016). Hence, extensional strain axes are dominant in central and eastern parts of the Weihe Basin region.

An interesting phenomenon between the principal strain axes and the distribution of ground fissures can be seen in Fig. 3a–c. The ground fissures in the Weihe Basin are distributed mainly in several bands in central and eastern parts of the basin where extensional strain prevails. It indicates that the formation and the development of ground fissures are caused primarily by the activity of tectonic faults and that they are closely related to the regional tectonic stress field. In the short term (tens to hundreds of years), the strain inside the plate is close to the elastic strain; thus, the stress–strain field in the plate follows the elastic constitutive law and the principal stress axis coincides with the principal strain axis at any point (Reynolds et al., 2002). The direction of tensile strain is approximately vertical to the faults (and ground fissures), showing that tensile stress drives the development of the numerous ground fissures (Zhang et al., 2011). Furthermore, the difference in the tectonic strain field is also the fundamental reason for the heterogeneous development of ground fissures in eastern and western parts of the Weihe Basin (Zhang et al., 2012).

5.2. Variations of the maximum shear strain and their correlation with seismicity

The magnitude of the shear strain rate reflects the degree of crustal deformation, i.e., the higher the shear strain rate, the more severe the crustal activity. Generally, higher rates of strain accumulation should be associated with larger or more frequent earthquakes (Segall, 2010). To obtain the spatial distribution of maximum shear strain rate for analysis of its correlation with seismicity, the maximum shear strain rate at any location of the study region was obtained by Kriging interpolation. Contour maps of the maximum shear strain rate were constructed based on the eigenvalues of the strain rates. The maximum shear strain rates over the study area, during the three studied periods, together with the major faults (green lines) and earthquake activity (red circles) are illustrated in Fig. 4a–c. The contour map for 2001–2007 (Fig. 4a) shows that the entire southern portion of the Weihe Basin region possessed higher maximum shear strain rates than northern parts, with the maximum value reaching 2.8×10^{-8} /yr in the southwest of the study area. Then, during 2008–2011, the southeastern Weihe Basin region displayed values of maximum shear strain rates markedly higher than northwestern parts (Fig. 4b), with the maximum value reaching 3.9×10^{-8} /yr. However, during 2007–2008, the entire region was subject to higher maximum shear strain rates, with a distribution trend exactly opposite to 2008–2011. The contour map of the southwestern Weihe Basin region shows higher maximum shear strain rates than northeastern parts (Fig. 4c), with the maximum value reaching about 8.4×10^{-8} /yr.

The contour maps of the maximum shear strain rates indicate that crustal activity in southern parts of the Weihe Basin region was stronger than in northern areas during 2001–2007. Consequently, we find that more earthquakes occurred in southern parts of the Weihe Basin region during 2001–2007 than in northern parts (Fig. 4a). The same can be seen during 2008–2011 (Fig. 4b) and 2007–2008 (Fig. 4c), i.e., areas with higher shear strain rates correspond to areas with more earthquakes. The contour maps indicate correlation between the maximum shear strain field and the distribution of seismicity, i.e., regions with high shear strain are generally areas with frequent earthquakes. However, earthquakes also occurred in areas with lower shear strain rates, e.g., northern (Fig. 4a), southwestern (Fig. 4b), and southeastern (Fig. 4c) parts of the Weihe Basin region. The reason might be that these areas lack any GPS observations or sufficient GPS observations to generate relatively precise shear strain maps. Additionally, almost all the earthquakes that occurred within the Weihe Basin during 2001–2011 were very small (Ml < 3.0), with only one relatively large earthquake (the 2009 Ml 4.4 Jingyang earthquake). Overall, the maximum shear rates transferred from southern parts of the Weihe Basin before 2008 (Fig. 4a) to southwestern parts during 2008 (Fig. 4c), then to eastern parts after 2008 (Fig. 4b), suggesting the effect of the northeastward extrusion caused by the Wenchuan earthquake.

To analyze further the possible influence of the Wenchuan earthquake on the seismicity of the Weihe Basin region in 2008, we divided the year into a pre-earthquake period (January–April) and a post-earthquake period (May–August). Based on the distribution of earthquakes, it is obvious that fewer earthquakes occurred during January–April (Fig. 5a), and those that did occur were concentrated in eastern parts of the Weihe Basin region. From May–August (Fig. 5b), not only was there a considerable increase in seismicity but the earthquakes were distributed more heavily in western parts of the Weihe Basin region. This might indicate that the increased earthquake activity in western parts of the Weihe Basin region was influenced by the Wenchuan earthquake, which also caused short-term compressional strain fields in this region (Figs. 3c and 4c).

It should be noted that the postseismic effect of the Wenchuan earthquake was not considered in the GPS velocities during the period 2008–2011. According to Ding et al. (2013), the main postseismic displacements were concentrated within ~50 days after the mainshock and they rapidly decayed with distance (Cui et al., 2016). Therefore, it was considered that the postseismic displacements did not exert great influence on the average velocities (2008–2011) in our study area. If there were continuous GPS or other geodetic observations, we could further distinguish the detailed deformation information to enhance the results presented here. Furthermore, we analyzed only the correlation between seismicity and maximum shear strain rates based mainly on the degree of crustal activity. In fact, the processes of the development and the occurrence of earthquakes are complex. In future work involving the seismology and a suitable focal mechanism, inversion methods will be combined to explore the mechanism(s) of earthquakes in the Weihe Basin region.

The strain results obtained in this study showed no obvious correlation with the faults. The main purpose behind the construction of the GPS monitoring network was to investigate regional crustal movements and deformations of the Weihe Basin and surrounding areas. The GPS sites are positioned in reasonably stable areas far from any fault zone (Fig. 2). Therefore, although the GPS velocity fields can represent regional crustal movements, there are too few GPS sites near faults to characterize their movements. In addition, the numerical finite element analysis method showed the current average velocity of the regional faults is about 1 mm/yr (Qu et al., 2017). Therefore, there is no obvious relationship between the strain field and the faults. If the network of GPS sites was denser across the faults, the correlation between the crustal deformation characteristics calculated by the GPS velocities and the activity of the tectonic faults might be elucidated.

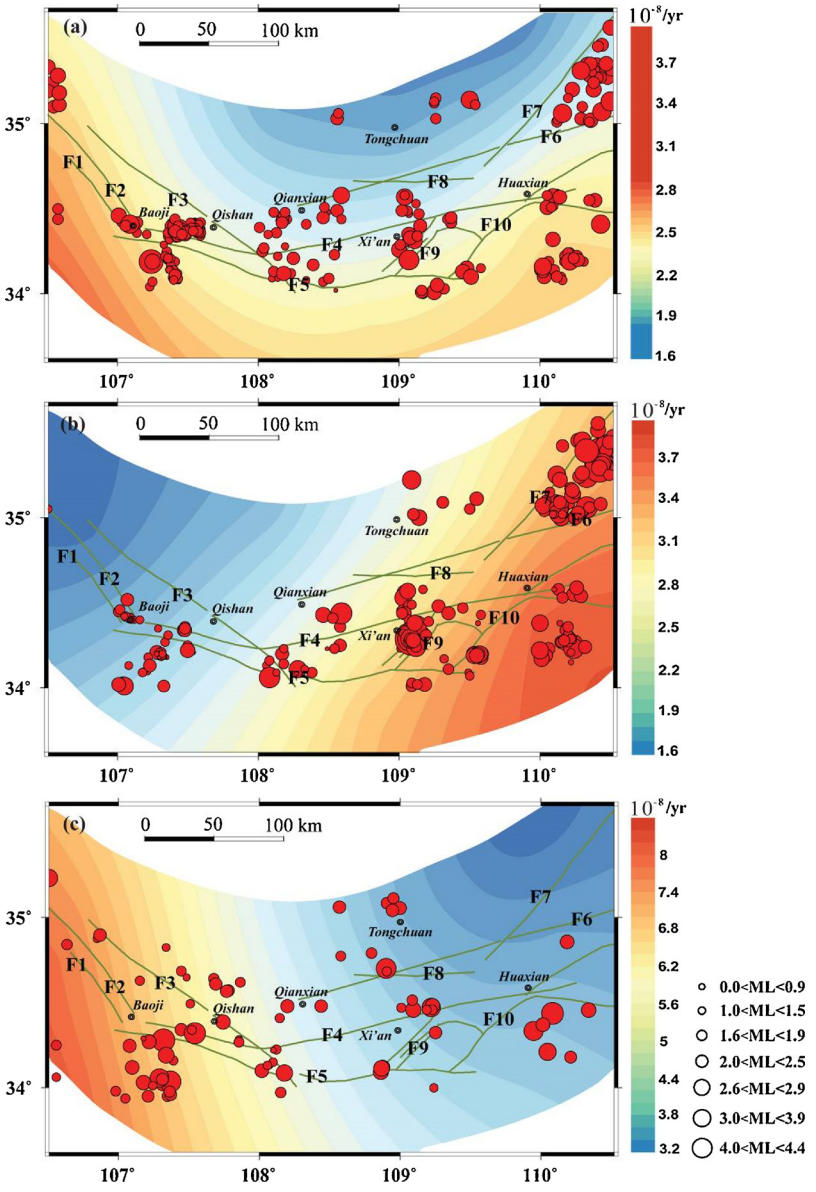

Fig. 4. Contour maps of the maximum shear strain rates (unit:10^{-8}/yr) and the distribution of earthquakes over the Weihe basin region, during the periods of 2001–2007 (Fig. 4a), 2008–2011 (Fig. 4b) and 2007–2008 (Fig. 4c), respectively. The detailed seismic statistical records are from the Shaanxi Seismic Information Network and the China Seismic Network (http://www.ceic.ac.cn, http://www.eqsn.gov.cn).

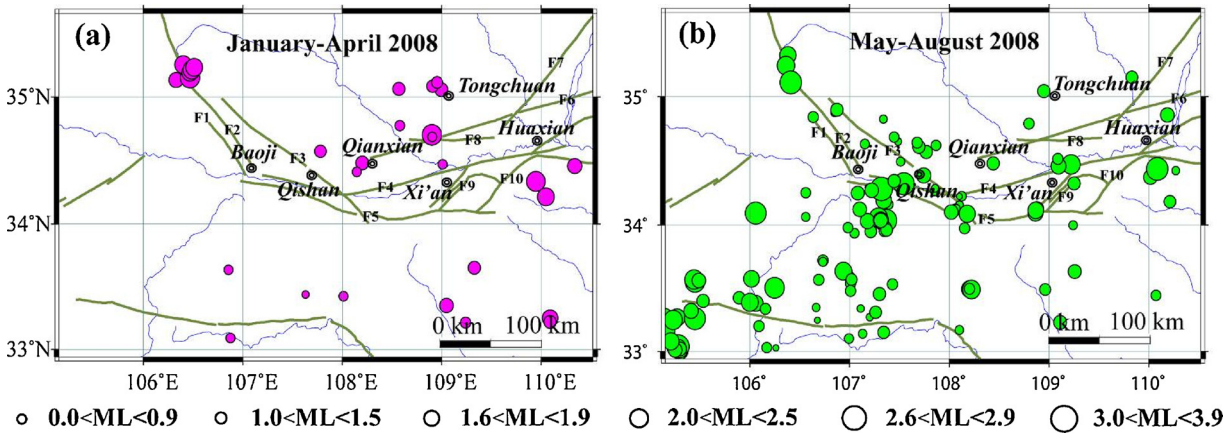

Fig. 5. The distribution of earthquakes in 2008 in the Weihe basin region before and after the Wenchuan earthquake from January to April (Fig. 5a) and from May to August (Fig. 5b) in 2008, respectively. The epicenter of the main Wenchuan earthquake event occurred approximately 500 km to the southwest of the study area.

Finally, the strain features presented here are consistent with the recent geodynamic background, geological and geophysical surveys (discussed in Section 5.1), and the formation mechanism of tectonic ground fissures. In addition, the GPS measurements provide important insight for investigating active deformation of the crust. Because the GPS data record indicates a predominantly interseismic strain pattern, one must wonder about the location of the release of the GPS-predicted strain. The Weihe Basin is an active basin in which several great historic earthquakes have occurred. This indicates that active deformation of the crust should be reasonably strong within the basin. Correspondingly, our results showed that the highest values of active deformation were found mostly within the Weihe Basin.

6. Conclusions

This study used GPS observations from yearly campaigns during 2001–2011 to analyze the variations of the crustal deformation and the strain field of the Weihe Basin region. Despite some fluctuation in the degree of crustal movement in the short term, the overall crustal movement of the entire Weihe Basin region was found temporally continuous during our observation period. The entire Weihe Basin region exhibited an overall tendency of movement toward the southeast with respect to the stable Eurasian Plate. Although the principal strain rates of the Weihe Basin region showed some short-term variations, the overall features of the principal strain field were not altered in the long term. It was found that western and eastern parts of the Weihe Basin region presented compressional and extensional strains, respectively.

We found correlation between the maximum shear strain field and the distribution of seismicity, i.e., regions with high shear strain were also areas with frequent earthquakes. In addition, there was an obvious increase in seismicity in western parts of the Weihe Basin region during May–August 2008 following the Wenchuan earthquake.

According to the variation characteristics of the crustal deformation and the strain fields, we inferred that western parts of the Weihe Basin region might have been affected during 2007–2008 by a northeastward extrusion caused by the Wenchuan earthquake. However, over time, this dynamic effect might have gradually permeated to eastern parts of the Weihe Basin region during 2008–2011. The findings of this study will enhance the understanding of the current tectonic deformation characteristics and recent geodynamic processes of the Weihe Basin region. Our future studies will continue the monitoring of the crustal movements in the study region using GPS technology (additional continuous GPS) and other monitoring sensors such as interferometric synthetic aperture radar, gravity monitoring, and leveling techniques to improve the resolution and accuracy of the monitoring capability.

Acknowledgements

The authors are grateful to surveyors who work hard to obtain GPS data in the challenging environment of the Weihe basin region. We thank the Second Monitoring Center of China Earthquake Administration and the Earthquake Administration of Shaanxi province for providing the high precision GPS data and assistance. This work was supported by the China Scholarship Fund of China Scholarship Council (CSC), the Nature Science Fund of China (NSFC) (Grant Nos. 41731066, 41674001, 41790445, 41604001, 41202189, 41504005), the Natural Science Basic Research Plan in Shaanxi Province of China (Grant No. 2016JM4005), the China Postdoctoral Science Foundation (Grant Nos. 2013M530412, 2016M602741), the Special Fund for Basic Scientific Research of Central Universities (No. CHD300102268204, CHD310826172202) and the Shuler-Foscue Endowment at Southern Methodist University. Constructive comments from Editor Volker Klemann and two anonymous reviewers have significantly improved the manuscript. Some figures were prepared using the public domain Generic Mapping Tools GMT (Wessel and Smith, 1998).

References

Altamimi, Z., Collilieux, X., Metivier, L., 2011. ITRF2008: an improved solution of the international terrestrial reference frame. J. Geod. 85 (8), 457–473. http://dx.doi.org/10.1007/s00190-011-0444-4.

Bai, C.Y., Peng, J.P., Greenhalgh, S., 2008. 3-D P-wave velocity structure of the crust beneath the Loess Plateau and surrounding regions of China. Tectonophysics 460, 278–287. http://dx.doi.org/10.1016/j.tecto.2008.08.027.

Bai, D.H., Unsworth, M.J., Meju, M.A., 2010. Crustal deformation of the eastern Tibetan plateau revealed by magnetotelluric imaging. Nat. Geosci. 3 (5), 358–362. http://dx.doi.org/10.1038/ngeo830.

Bao, X., Xu, M., Wang, L., Mi, N., Yu, D., Li, H., 2011. Lithospheric structure of the Ordos Block and its boundary areas inferred from Rayleigh wave dispersion. Tectonophysics 499, 132–141. http://dx.doi.org/10.1016/j.tecto.2011.01.002.

Burbidge, D.R., 2004. Thin plate neotectonic models of the Australian plate. J. Geophys. Res.: Solid Earth 109 (B10), 1978–2012.

Calais, E., Galisson, L., Stephan, J.F., Delteil, J., Deverchere, J., Larroque, C., Mercier, B., Popoff, M., Sosson, M., 2000. Crustal strain in the Southern Alps, France, 1948-1998. Tectonophysics 319, 1–17. http://dx.doi.org/10.1016/S0040-1951(00)00029-9.

CENC, 2007. China earthquake networks center). The 1556 Huaxian Great Earthquake, Shaanxi, China: The Largest Total of Fatalities Ever Claimed. (in Chinese).

Chen, H., Hu, J.M., Wu, G.L., Shi, W., Geng, Y.Y., Qu, H.J., 2015. Apatite fission-track thermochronological constraints on the pattern of late Mesozoic–Cenozoic uplift and exhumation of the qinling orogen, central China. J. Asian Earth Sci. 114, 649–673. http://dx.doi.org/10.1016/j.jseaes.2014.10.004.

Cui, D.X., Hao, M., Li, Y.H., Wang, W.P., Qing, X.L., Li, C.J., 2016. Present-day crustal movement and strain of the surrounding area of Ordos block derived from repeated GPS observations. Chin. J. Geophys. 59 (10), 3646–3661 (in Chinese with English abstract).

Dai, W.Q., Ren, J., Zhao, X.M., Shao, H.C., Zhu, G.Z., 2004. Characteristics of horizontal crustal movement in Weihe Basin and adjacent zones by GPS observation. Acta Seismol. Sin. 26 (3) 256-26 (in Chinese with English abstract).

Deng, Q., 2007. Active Tectonics Map of China. Seismological Press (in Chinese).

Ding, K.H., Xu, C.J., Wen, Y.M., 2013. Postseismic deformation associated with the 2008 Wenchuan earthquake by GPS data. Geomatics Inf. Sci. Wuhan Univ. 38 (2), 131–135 (in Chinese with English abstract).

Dong, D., Herring, T., King, R., 1998. Estimating regional deformation from a combination of space and terrestrial geodetic data. J. Geod. 72, 200–214. http://dx.doi.org/10.1007/s001900050161.

Dong, D., Fang, P., Bock, Y., Webb, F., Prawirodirdjo, L., Kedar, S., Jamason, P., 2006. Spatiotemporal filtering using principal component analysis and karhunen-love expansion approaches for regional GPS network analysis. J. Geophys. Res. 111, B03405. http://dx.doi.org/10.1029/2005JB003806.

Feng, X., Tian, Q., Sheng, X., 2003. Analysis of activity difference of the west section of the weihe fault. Geol. Rev. 49, 233–238 (in Chinese with English abstract).

Gan, W.J., Zhang, P.Z., Shen, Z.K., Niu, Z.J., Wang, M., Wan, Y.G., Zhou, D.M., Cheng, J., 2007. Present-day crustal motion within the tibetan plateau inferred from GPS measurements. J. Geophys. Res.: Solid Earth 112, B08416. http://dx.doi.org/10.1029/2005JB004120.

Gao, G.M., Kang, G.F., Li, G.Q., Bai, C.H., 2015. Crustal magnetic anomaly in the Ordos region and its tectonic implications. J. Asian Earth Sci. 109, 63–73. http://dx.doi.org/10.1016/j.jseaes.2015.04.033.

Guo, Z.G., Chen, Y.J., 2016. Crustal structure of the eastern qinling orogenic belt and implication for reactivation since the cretaceous. Tectonophysics 683, 1–11. http://dx.doi.org/10.1016/j.tecto.2016.06.007.

Hackl, M., Malservisi, R., Wdowinski, S., 2009. Strain rate patterns from dense GPS networks. Nat. Hazards Earth Syst. Sci. 9, 1177–1187. http://dx.doi.org/10.5194/nhess-9-1177-2009.

Herring, T.A., 2002. GLOBK: Global Kalman Filter VLBI and GPS Analysis Program, Version 10.0. Massachusetts Institute of Technology, Cambridge.

Hori, M., 2003. Stress inversion method for predicting local stress distribution of body in two dimensional state of plane stress or strain. Mech. Mater. 35, 395–406. http://dx.doi.org/10.1016/S0167-6636(02)00256-9.

Jiang, W.L., Xiao, Z.M., Xie, X.S., 2000. Segmentations of active normal dip-slip faults around Ordos block according to their surface ruptures in historical strong earthquakes. Earthq. Sci. 13 (5), 552–562.

Jiang, L., Qiu, Z., Wang, Q.H., Guo, Y.S., Wu, C.F., Wu, Z.J., Xue, Z.H., 2016. Joint development and tectonic stress field evolution in the southeastern mesozoic Ordos Basin, west part of North China. J. Asian Earth Sci. 127, 47–62. http://dx.doi.org/10.1016/j.jseaes.2016.06.017.

King, R.W., Bock, Y., 2000. Documentation for the GAMIT GPS Analysis Software, Release 10.0. Massachusetts Institute of Technology, Cambridge.

Koch, K.R., 1980. Parameterschatzung und hypothesen tests in linearen modellen. Bonn: Dummler. .

Kogan, M.G., Steblov, G.M., King, R.W., et al., 2000. Geodetic constraints on the rigidity and relative motion of Eurasia and North America. Geophys. Res. Lett. (14), 27.

Kuo, T., 1957. On the Shensi earthquake of january 23, 1556. Acta Geophys. Sin. 6, 59–68 (in Chinese with English abstract).

Li, Y.X., Zhang, J.H., He, J.K., 2007. Current day tectonic motion and intraplate deformation strain field obtained from space geodesy in the Pacific Plate. Chin. J. Geophys. 50 (2), 437–447 (in Chinese with English abstract).

Li, D.P., Du, J.J., Ma, Y.S., Xiao, A.F., 2015. Active faults and dip slip rates along the northern margins of the Huashan Mountain and Weinan loess tableland in the southeastern Weihe Graben, central China. J. Asian Earth Sci. 114, 266–278. http://dx.doi.org/10.1016/j.jseaes.2015.08.013.

Li, M.K., Zhang, S.X., Wang, F., Wu, T.F., Qin, W.B., 2016. Crustal and upper-mantle structure of the southeastern Tibetan Plateau from joint analysis of surface wave dispersion and receiver functions. J. Asian Earth Sci. 117, 52–63. http://dx.doi.org/10.1016/j.jseaes.2015.12.002.

Lin, A., Rao, G., Yan, B., 2015. Flexural fold structures and active faults in the northern-

western Weihe Graben, Central China. J. Asian Earth Sci. 114, 226–241. http://dx.doi.org/10.1016/j.jseaes.2015.04.012.
Liu, M., Wang, H., 2012. Roaming earthquakes in China highlight mid-continental hazards. EOS, Trans. Am. Geophys. Union 93 (45), 453–464.
Liu, M., Yang, Y.Q., Shen, Z., Wang, S., Wang, M., Wan, Y., 2007. Active tectonics and intra-continental earthquakes in China: the kinematics and geodynamics. In: Stein, S., Mazzotti, S. (Eds.), Continental Intraplate Earthquakes: Science, Hazard, and Policy Issues: Geological Society of America Special Paper 425, pp. 299–318. http://dx.doi.org/10.1130/2007.2425(19.
Liu, J.H., Zhang, P.Z., Lease, R.O., Zheng, D.W., Wan, J.L., Wang, W.T., Zhang, H.P., 2013. Eocene onset and late miocene acceleration of Cenozoic intracontinental extension in the North Qinling range–Weihe graben: insights from apatite fission track thermochronology. Tectonophysics 584, 281–296. http://dx.doi.org/10.1016/j.tecto.2012.01.025.
Liu, J.W., Xie, F.R., Lv, Y.J., 2016. Seismic hazard assessments for the Ordos block and its periphery in China. Soil. Dyn. Earthq. Eng. 84, 70–82. http://dx.doi.org/10.1016/j.soildyn.2016.02.007.
Mercier, J.L., Vergely, P., Zhan, Y.Q., Hou, M.J., Bellier, O., Wang, Y.M., 2013. Structural records of the late Cretaceous-Cenozoic extension in Eastern China and the kinematics of the Southern Tan-Lu and Qinling fault zone (Anhui and Shaanxi provinces, PR China). Tectonophysics 582 (2), 50–75. http://dx.doi.org/10.1016/j.tecto.2012.09.015.
Myers, J.R., Gomez, F.G., 2010. Analysis of Subsidence and Ground Fissuring in the FenWei Basin (Northern China) Using Radar Interferometry. AGU Fall Meeting Abstracts#H23F-1297.
Nanjo, K.Z., Turcotte, D.L., Shcherbakov, R., 2005. A model of damage mechanics for the deformation of the continental crust. J. Geophys. Res.: Solid Earth 110 (B7), 1979–2012.
Northrup, C.J., Royden, L.H., Burchfiel, B.C., 1995. Motion of the Pacific plate relative to Eurasia and its potential relation to Cenozoic extension along the easternmargin of Eurasia. Geology 23, 719–722.
Pan, S.Z., Niu, F.L., 2011. Large contrasts in crustal structure and composition between the Ordos plateau and the NE Tibetan plateau from receiver function analysis. Earth Planet. Sci. Lett. 303, 291–298. http://dx.doi.org/10.1016/j.epsl.2011.01.007.
Peng, J., 1992a. Tectonic evolution and seismicity of Weihe fault zone. Seismol. Geol. 14, 113–120 (in Chinese with English abstract).
Peng, J.B., Zhang, J., Su, S.R., 1992b. The Activity Faults and Ground Fissures Disaster of Weihe Basin. Northwestern University Press, Xi'an (in Chinese).
Peng, J.B., Chen, L.W., Huang, Q.B., 2013. Physical simulation of ground fissures triggered by underground fault activity. Eng. Geol. 155, 19–30. http://dx.doi.org/10.1016/j.enggeo.2013.01.001.
Qu, W., Zhang, Q., Wang, Q.L., Lin, Qing., 2009. Research on horizontal crustal motion and strain features of Weihe basin with GPS data. J. Geod. Geodyn. 29 (4), 34–37 (in Chinese with English abstract).
Qu, W., Zhang, Q., Wang, Q.L., Li, Z.H., 2011. Research on present crustal horizontal deformation feature of weihe basin and its tectonic activity. Geomatics Inf. Sci. Wuhan Univ. 36 (7), 830–834 (in Chinese with English abstract).
Qu, F.F., Zhang, Q., Lu, Z., Zhao, C.Y., Yang, C.S., Zhang, J., et al., 2014a. Land subsidence and ground fissures in Xi'an, China 2005–2012 revealed by multi-band InSAR time-series analysis. Remote Sens. Environ. 155, 366–376. http://dx.doi.org/10.1016/j.rse.2014.09.008.
Qu, W., Lu, Z., Zhang, Q., Li, Z.H., Peng, J.B., Wang, Q.L., Drummond, J., Zhang, M., 2014b. Kinematic model of crustal deformation of fenwei Basin, China based on GPS observations. J. Geodyn. 75, 1–8. http://dx.doi.org/10.1016/j.jog.2014.01.001.
Qu, W., Wang, Y.S., Xu, C., Zhang, Q., Wang, Q.L., 2017. Current tectonic stress and activities characteristics of the deep fault within Weihe basin. Geomatics Inf. Sci. Wuhan Univ. 42 (6), 825–830. http://dx.doi.org/10.13203/j.whugis20140744.
Rao, G., Lin, A., Yang, B., Jia, D., Wu, X.J., 2014. Tectonic activity and structural features of active intracontinental normal faults in the Weihe Graben, central China. Tectonophysics 636, 270–285. http://dx.doi.org/10.1016/j.tecto.2014.08.019.
Reddy, J.N., 2013. An Introduction to Continuum Mechanics, 2nd ed. Cambridge University Press, NewYork.
Ren, J., Peng, J.B., Wang, F.Y., et al., 2012. The research of deep structural features of Weihe basin and adjacent areas. Chin. J. Geophys. 55 (9), 2939–2947. http://dx.doi.org/10.6038/j.issn.0001-5733.2012.09.013. (in Chinese).
Ren, J., Feng, X.J., Wang, F.Y., 2013. Revealed the fine crust structures of Xi'an sag in Weihe basin by deep seismic reflection profile. Chin. J. Geophys. 56, 513–521. http://dx.doi.org/10.6038/cjg20130215. (in Chinese with English Abstract).
Reynolds, S.D., Coblentz, D.D., Hillis, R.R., 2002. Tectonic forces controlling the regional intraplate stree field in continental Australia: results from new finite element modeling. J. Geophus. Res. 107 (B7), 2131. http://dx.doi.org/10.1029/2001JB000408.
Riguzzi, F., Crespi, M., Devoti, R., Doglioni, C., Pietrantonio, G., Pisani, A.R., 2012. Geodetic strain rate and earthquake size: new clues for seismic hazardstudies. Phys. Earth Planet. Int. 206–207, 67–75. http://dx.doi.org/10.1016/j.pepi.2012.07.005.
Royden, L.H., et al., 2008. The geological evolution of the Tibetan plateau. Science 321, 1054.
Savage, J.C., Can, W., Svarc, J.L., 2001. Strain accumulation and rotation in the Eastern California Shear Zone. J. Geophys. Res. 106 (B10), 21995–22007. http://dx.doi.org/10.1029/2000JB000127.
Schellart, W.P., Freeman, J., Stegman, D.R., Moresi, L., May, D., 2007. Evolution and diversity of subduction zones controlled by slab width. Nature 446, 308–311.
Segall, P., 2010. Earthquake and Volcano Deformation. Princeton University Press, New Jersey/Oxfordshire.
Shen, Z.K., Zhao, C.K., Yin, A., Li, Y.X., David, D.J., Fang, P., Dong, D.N., 2000. Contemporary crustal deformation in east Asia constrained by global positioning system measurements. J. Geophys. Res.: Solid Earth 105 (B3), 5721–5734. http://dx.doi.org/10.1029/1999JB900391.
Shen, Z.K., Sun, J.B., Zhang, P.Z., 2009. Slip maximum at fault junctions and rupturing of barriers during the 2008 Wenchuan earthquake groups. Nat. Geosci. 2 (10), 718–724. http://dx.doi.org/10.1038/ngeo636.
Shi, Y.Q., Feng, X.J., Dai, W.Q., et al., 2008. Distribution and structural characteristics of the Xi'an section of the Weihe fault. Acta Seismol. Sin. 30 (6), 634–647.
SMCCEA, 2013. China Comprehensive Geophysical Field Observation- Project of the Surrounding Areas of the Ordos Block. Second Monitoring Center, China Earthquake Administration, Xi'an, Shaaxi province, China (in Chinese).
Song, L.S., 1989. The Earthquake Records of Shanxi. Earthquake Press, Beijing (in Chinese).
SSB, 1988. State seismological Bureau. Active Fault System Around Ordos Massif. Seismological Press, Beijing, pp. 352 (in Chinese).
Tao, B.Z., 2007. The Statistical Theory and Methods of the Survey Measurement Data Processing. Surveying and Mapping Press (in Chinese with English abstract).
Tian, Q., Shen, X., Feng, X., Wei, K., 2003. Primary study on quaternary tectonic events based on variation of fault activity in Weihe basin. Seismol. Geol. 25, 146–154 (in Chinese with English abstract).
Wakita, K., Pubellier, M., Windley, B.F., 2013. Tectonic processes, from riffing to collision via subduction, in SE Asia and the western Pacific: a key to understanding the architecture of the cential Asian orogenic belt. Lithosphere 5 (3), 265–276.
Wang, J., 1980. Ground ruptures during the large earthquake of 1556, Huaxian County. Shanxi. Acta Seismol. Sin. 2, 430–437 (in Chinese with English abstract).
Wang, M., 2009. Analysis of GPS Data With High Precision and Study on Present-Day Crustal Deformation in China. PhD Thesis (in Chinese with English abstract). .
Wang, W.D., 2010. Study on the Regional Stability Dynamical Background in the Forming of Xi'an Ground Fissures. PhD, Thesis. Xi'an: Chang'an University.
Wang, K.Y., Ma, J., Diao, G.L., 2012. Present day stress state of the Shanxi tectonic belt. Geodyn. Tectonophys. 3 (3), 195–202. http://dx.doi.org/10.5800/GT-2012-3-3-0071.
Wang, C.Y., Sandvol, E., Zhu, L., Lou, H., Yao, Z.X., Luo, X.H., 2014. Lateral variation of crustal structure in the Ordos block and surrounding regions, North China, and its tectonic implications. Earth Planet. Sci. Lett. 387, 198–211. http://dx.doi.org/10.1016/j.epsl.2013.11.033.
Ward, S.N., 1994. A multidisciplinary approach to seismic hazard in southern California. Bull. Seismol. Soc. Am. 84 (5), 1293–1309.
Wessel, P., Smith, W.H.F., 1998. New, improved version of generic mapping tools released. EOS Trans. AGU 79, 579.
White, L.T., Lister, G.S., 2012. The collision of India with Asia. J. Geodyn. (56-57), 7–17. http://dx.doi.org/10.1016/j.jog.2011.06.006.
Wu, Y.Q., Jiang, Z.S., Zhao, J., Liu, X.X., Wei, W.X., Liu, Q., Li, Q., Zou, Z.Y., Zhang, L., 2015. Crustal deformation before the 2008 Wenchuan Ms8.0 earthquake studied using GPS data. J. Geodyn. 85, 11–23. http://dx.doi.org/10.1016/j.jog.2014.12.002.
Xie, Y., 1992. On magnitude of 1556 Guanzhong great earthquake. J. Catastrophol. 7, 10–13 (in Chinese with English abstract).
Xie, Z.Q., Fang, J.A., Tian, X.T., et al., 1991. The evolution of the structural stress field and analysis of the formation mechanism in the weihe basin. J. Xi'an. Coll. Geol. 12 (1), 46–52 (in Chinese with English abstract).
Xu, Y.J., Shen-tu, B.M., Wang, Y.P., 1988. A preliminary study of the characteristics of the activity of the northern boundary fault belt of Weihe basin. Seismol. Geol. 10, 77–88 (in Chinese with English abstract).
Xu, C.J., Wang, J.J., Li, Z.H., 2010. Applying the Coulomb failure function with an optimally oriented plane to the 2008 Mw 7.9 Wenchuan earthquake groups triggering. Tectonophysics 491 (1–4), 119–126. http://dx.doi.org/10.1016/j.tecto.2009.09.019.
Yang, M.H., Li, L., Zhou, J., Qu, X.Y., Zhou, D., 2013. Segmentation and inversion of the Hangjinqi fault zone, the northern Ordos basin (North China). J. Asian Earth Sci. 70–71, 64–78. http://dx.doi.org/10.1016/j.jseaes.2013.03.004.
Zhang, Y.Q., Mercier, J.L., Vergdly, P., 1998. Extension in the graben systems around the Ordos (China), and its contribution to the extrusion tectonics of south China with respect to Gobi-Mongolia. Tectonophysics 285, 41–75.
Zhang, Y.Q., Ma, Y.S., Yang, N., Shi, W., Dong, S.W., 2003. Cenozoic extensional stress evolution in North China. J. Geodyn. 36 (5), 591–661. http://dx.doi.org/10.1016/j.jog.2003.08.001.
Zhang, P.Z., Gan, W.J., Shen, Z.K., 2005. A coupling model of rigid-block movement and continuous deformation: patterns of the present-day deformation of China' s continent and its vicinity. Acta Geol. Sin. 79 (6), 748–756 (in Chinese with English abstract).
Zhang, Q., Qu, W., Wang, Q.L., Peng, J.B., Drummond, J., Li, Z.H., Lin, Q., 2011. Analysis of present tectonic stress and regional ground fissure formation mechanism of the Weihe Basin. Surv. Rev. 43http://dx.doi.org/10.1179/003962611X13055561708740. 382-38.
Zhang, Q., Qu, W., Peng, J.B., 2012. Research on tectonic causes of numerous ground fissures development mechanism and its unbalance distribution between eastern and western of Weihe basin. Chin. J. Geophys. 55 (8), 2589–2597. http://dx.doi.org/10.6038/j.issn.0001-5733.2012.08.010. (in Chinese with English abstract).
Zhou, Y., Liang, X.Q., Krner, A., Cai, Y.F., Shao, T.B., Wen, S.N., Jiang, Y., Fu, J.G., Wang, C., Dong, C.G., 2015. Late Cretaceous lithospheric extension in SE China: constraints from volcanic rocks in Hainan Island. Lithos 232, 100–110. http://dx.doi.org/10.1016/j.lithos.2015.06.028.